RESEARCH

Feasibility Study of Measuring Degree of Linear Polarization of the Solar F-Corona Using Filter Observations on the COronal Diagnostic EXperiment

Heesu Yang[1] · Kyuhyoun Cho[2,3] · Su-Chan Bong[1] · Seonghwan Choi[1] ·
Maria S. Madjarska[4,5] · Yeon-Han Kim[1] · Nelson Reginald[6] · Jeffrey Newmark[6]

Abstract

One of the most unrevealed pieces of information about solar F-corona is its polarization. We propose the possibility of measuring the degree of linear polarization (D_F) of the F-corona along the radial distance from the Sun using the signal of two filters installed on the COronal Diagnostic EXperiment (*CODEX*), which will be mounted on board the International Space Station in December 2023. By analyzing the signal and noise of *CODEX* with Monte-Carlo simulations, we can derive D_F with a 1.4 nm-width narrow bandpass filter centered at 393.55 nm and a 10 nm-width broad bandpass filter centered at 393.5 nm by stacking six images and integrating over $1\,R_\odot \times 1\,R_\odot$. The D_F measured by *CODEX* will help reduce the uncertainty of the K-coronal polarization (pB_K), a main target of the mission, as well as to provide a better understanding of the F-corona.

1. Introduction

Solar F-corona is the light caused by the scattering of interplanetary dust particles (IDPs) between the Sun and the Earth. Its spectrum shows Fraunhofer lines rather than the continuum because the motion of IDPs is slow, so the spectrum keeps the absorption shape of the solar photosphere. This is the main difference compared to the continuum spectrum of the K-corona caused by Thomson scattering from free electrons.

The lower K- and F-corona have been observed during total solar eclipses (TSE; van de Hulst, 1950; Blackwell and Petford, 1966; Koutchmy and Lamy, 1985; Cho et al., 2020; Boe et al., 2021; Hanaoka, Sakai, and Takahashi, 2021). The TSE ground observations have mainly been made within 5 $R_\odot$ due to the sky brightness of about $10^{-9}\,I_\odot$ (solar disk brightness). This sky brightness is comparable with the photon noise level of the coronal signal at 5 $R_\odot$ in most of the TSE observations. The observations of the outer corona beyond 5 $R_\odot$ have only been conducted by satellites such as the *Large Angle and Spectrometric Coronagraph* (*LASCO*) and the *Solar TErrestrial RElations Observatory* (*STEREO*).

The source of the F-corona is most likely the light scattering from IDPs evaporating from the comets or asteroids approaching the Sun (Mann, 1998; Yang and Ishiguro, 2015). The

---

Extended author information available on the last page of the article

scattering, however, cannot be expressed mathematically because IDPs have irregular shapes (Zubko et al., 2006). There exists an analytical solution of a single spherical particle known as Mie scattering (Mie, 1908), which is different from a real particle shape. In addition, the observations of the F-corona are affected by the contribution function along the line-of-sight (van de Hulst, 1947; Mann, 1998), which is still poorly understood. The invariable brightness of the F-corona over the solar cycle may be due to the scattering from IDPs around the Earth (Morgan and Habbal, 2007).

It has been widely accepted that the shape of the F-corona is an axis-symmetric elliptical flattened disk in the plane-of-the-sky (Koutchmy and Lamy, 1985; Morgan and Habbal, 2007; Lamy et al., 2020; Boe et al., 2021; Llebaria et al., 2021). Approaching the Sun, the shape of the F-corona is likely more spherical compared to the zodiacal light (Kimura and Mann, 1998). The flattened disk shape is reasonable considering the extension of the F-corona to the zodiacal light, and the more spherical shape of the F-corona may imply that part of it is caused by IDPs near the Earth (Mann et al., 2004). The distribution of the F-corona is likely unchanged for a long time (Llebaria et al., 2021; Burtovoi et al., 2022) but is possibly affected by CMEs, the solar wind, or streamers (Ragot and Kahler, 2003; Morgan and Habbal, 2007).

Some of the poorly known properties of the F-corona are the polarized brightness (pB_F) and the degree of linear polarization (D_F). Although various authors have attempted to unravel D_F from observations, it still lacks understanding (Blackwell and Petford, 1966; Koutchmy and Lamy, 1985; Mann and MacQueen, 1993; Boe et al., 2021). Koutchmy and Lamy (1985) found that D_F increases from 0.03% at 5 $R_\odot$ to about 2% at 10 $R_\odot$ assuming invariant K-coronal polarization (pB_K) above 5 $R_\odot$. Blackwell and Petford (1966) attempted to extract D_F from the observed polarized light (pB_{K+F}) using the filter ratio of a narrow bandpass filter (NBF) and a broad bandpass filter (BBF) of the Hα line based on certain assumptions during two total solar eclipse observations from an airplane. They reported that the polarization from 5 to 16 $R_\odot$ smoothly increases from 0.05 to 0.7%. Recently, Morgan and Cook (2020) inferred D_F of about $6.6 \pm 0.9\%$ at $4-5.5$ $R_\odot$ using *LASCO-C2* observations, which is a value far larger than previously estimated by Koutchmy and Lamy (1985) and Blackwell and Petford (1966). From a recent zodiacal light study, Lasue, Levasseur-Regourd, and Renard (2020) deduced that only a few percent of the F-coronal light is polarized by extrapolating the polarization of the zodiacal light.

The D_F also highly depends on the contribution function along the line-of-sight. Assuming that the F-coronal light comes from near the Sun, the F-coronal signal observed in the direction of the low corona may be zero because the IDPs near the Sun can be sublimated or melted. But the F-coronal component will exist in the direction of the low corona, and part of the light will be polarized (Mann et al., 2004; Lamy et al., 2020) because of the F-coronal light generated by the strong forward scattering of the small IDPs near the Earth. This may be reasonable considering the Gegenschein, the enhanced backward scattering of the sunlight.

An ultimate method to distinguish pB_F from pB_K is by measuring the relative depth of the Fraunhofer lines of polarized light (Blackwell and Petford, 1966). In this study, we investigate the possibility of measuring the depth of the Fraunhofer lines and D_F using the observations of a NBF centered at 393.55 nm and a BBF centered at 393.50 nm of the *COronal Diagnostic EXperiment* (*CODEX*).

In Section 2, we introduce the *CODEX* instrumentations with the specifications used in the calculations. In Section 3, we develop the model of the coronal spectrum, including polarization and the mathematical methodology of the signal calculations to derive D_F. Section 4 shows the results of the Monte-Carlo calculations on the D_F measurement expected from *CODEX*. Finally, Section 5 outlines the summary and the discussion.

Table 1 *CODEX* optical parameters.

| Parameters	Symbol [unit]	Values
aperture area	A_{ap} [mm^2]	$\pi \times 25^2$
transmission of filters	t_{f}	see Figure 1
bandwidth of BBF	w_{b} [nm]	10 (see Figure 1)
bandwidth of NBF	w_{n} [nm]	1.4 (see Figure 1)
transmission of optics except filter	t_{optics}	0.80
quantum efficiency	QE	see Figure 2
camera gain	g [e-/DN]	2.62
exposure time	t_{exp} [sec]	90
readout noise	readout$_{\mathrm{rms,e}}$ [e-]	2.15
dark current noise at 21 °C	dark$_{\mathrm{e}}$ [e- sec^{-1}]	1.05
full well depth	[e-]	8919
(super) pixel resolution	[″]	12.8
extinction ratio	ext_{pol}	242.75
diffraction		see Figure 2
vignetting		see Figure 2

2. Instrumentation

CODEX is a mission that will install a next generation solar coronagraph at the International Space Station (ISS) in December 2023. The primary purpose of *CODEX* is to measure the density, temperature, and velocity of the electrons comprising the K-corona by employing five blue-ultraviolet BBFs. The bandwidths of the BBFs are 10 nm centered at 393.50, 405.00, and 430.00 nm for the temperature measurements, and 398.70 and 423.30 nm for the speed measurements. Other five filter positions are allocated for the NBF centered at 393.55 nm, a neutral density filter of the optical density of 10^{-6}, two clear window filters, and a full bandpass filter covering the $385 - 440$ nm wavelength range. The neutral density filters will be used to calibrate and prevent damage from direct sunlight when the instrument loses the Sun pointing.

The field of view of the coronagraph is from 3 to 8 $R_{\odot}$. Its aperture diameter is 5.0 cm, which is a bit larger than the *LASCO* aperture. One of the edge-technology of the mission is a polarization Complementary Metal-Oxide Semiconductor (CMOS) camera installed at the focal plane. The CMOS camera uses a Sony IMX253MZR sensor, which has a linear polarization mask in front of each pixel. Four pixels in a square, which have four different linear polarization masks, namely 0°, 45°, 90°, and 135°, compose a super-pixel. By a simple calculation, we can measure the linear polarization in each super-pixel (Reginald et al., 2017). The optical point spread function is made to encompass a full super-pixel. The polarization-masked CMOS camera has a disadvantage concerning its extinction ratio. The extinction ratio (ext_{pol}) is smaller than the normal linear polarizer so that the signal can be contaminated by crosstalk.

Table 1 shows the *CODEX* parameters used in the current calculations. Some come from mechanical or optical simulations, and some are measured using the qualification model of the camera. The transmissions (t_{f}) and the bandwidths (w_{b} and w_{n}) of the filters are measured using the flight models of the filters. We note that the transmission of the optics except filter t_{optics} is a wavelength-dependent parameter in a real situation, but here we use a constant value because it is not characterized yet as a function of wavelength.

Figure 1 Coronal polarized brightness spectrum of the K- and F-corona (pB_K and pB_F) at $7 R_\odot$. pB_K is derived using the electron density profile of Leblanc, Dulk, and Bougeret (1998). The expected polarized brightness (dash-dotted line) is a sum of pB_K (dotted line) and pB_F (dashed line). A dark-gray rectangular profile represents the transmission of the BBF centered at 393.50 nm with a bandwidth of 10 nm, and a light-gray profile represents the transmission of the NBF centered at 393.55 nm with a bandwidth of 1.4 nm.
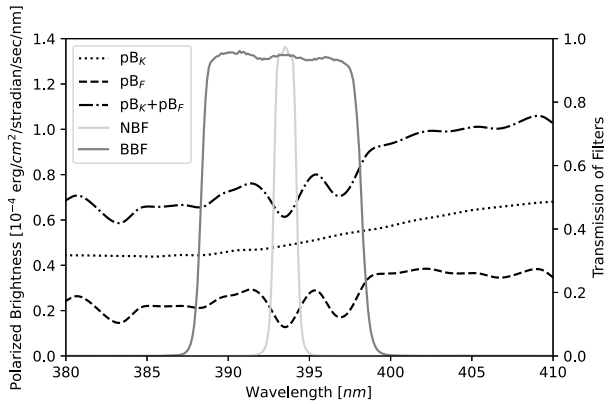
3. Methodology

To derive the linear polarization of the F-corona, D_F, we developed the approach described below. First, we adopt the calculation method of the total brightness (tB_K) and the polarized brightness (pB_K) of the K-corona of Cho et al. (2016) assuming coronal temperature and speed of $1\,000\,000$ K and 300 km s^{-1}, respectively, to mimic the solar coronal brightness. The coronal electron density profile of Leblanc, Dulk, and Bougeret (1998) is used in this calculation, rather than the profile of Baumbach (1937), which is used in Cho et al. (2016). We also adopt the pB_F from Koutchmy and Lamy (1985). We obtain the spectrum of tB_F and pB_F by multiplying with an air mass zero reference spectrum (ASTM, 2006).

Figure 1 shows the calculated pB spectrum of the K- (pB_K) and F-corona (pB_F) from 380 to 410 nm with the Ca II H & K lines at 393.4 and 396.8 nm, respectively. They are one of the strongest Fraunhofer lines near the blue end of the white-light band. The pB_K is flatter compared to the pB_F because the Thomson scattering smoothens the original spectrum irradiated from the photosphere. The dark-gray rectangular profile marks the broadband filter centered at 393.50 nm, which is fixed for the efficient measurement of the K-coronal electron temperature using the filters centered at 393.50, 405.00, and 430.00 nm.

The coronal light passes through the optical elements such as the bandpass filters, the lenses, and the mirrors. Using the model spectra, the number of electrons e_θ generated in a pixel of the CMOS sensor in a second can be calculated as

$$
\begin{aligned}
e_\theta = \int \Big\{ & \frac{t_f * t_{\text{optics}}}{E_{\text{ph},\lambda}} * QE_\lambda * A_{\text{ap}} * \Omega_{\text{pixel}} \\
& * (I_{t,\lambda} \cos^2\theta + I_{r,\lambda} \sin^2\theta + 0.5 * I_{\text{unpol},\lambda}) \\
& + \frac{t_f/ext_{\text{pol}} * t_{\text{optics}}}{E_{\text{ph},\lambda}} * QE_\lambda * A_{\text{ap}} * \Omega_{\text{pixel}} \\
& * (I_{t,\lambda} \sin^2\theta + I_{r,\lambda} \cos^2\theta + 0.5 * I_{\text{unpol},\lambda}) \Big\} \, d\lambda,
\end{aligned}
\tag{1}
$$

where $E_{\text{ph},\lambda}$ is the photon energy, A_{ap} is the aperture size of the optics, Ω_{pixel} is the solid angular size of a pixel, θ is the angle between the tangential direction and the linear polarization direction of the polarization mask, QE_λ is the quantum efficiency, and ext_{pol} is the extinction ratio of the polarization mask. $I_{t,\lambda}$ and $I_{r,\lambda}$ contain the tangential and radial com-
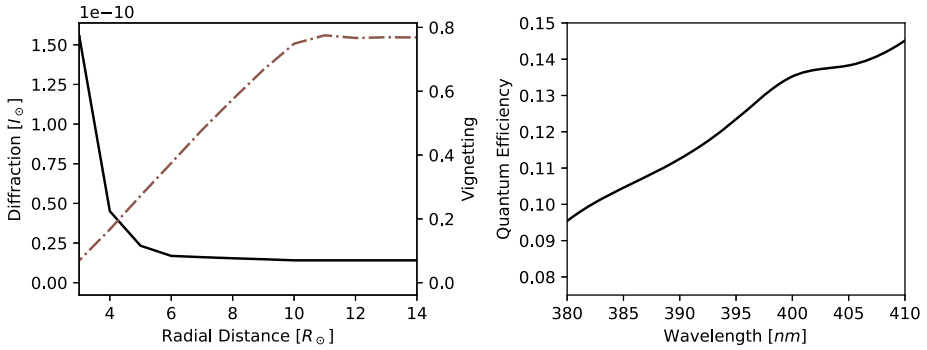
Figure 2 Diffraction and vignetting (left panel), and quantum efficiency (QE_λ, right panel) of the instrument used in the calculation. The black solid line in the left panel displays the diffraction over the radial distance, and the brown dash-dotted line shows the vignetting.

ponents of the K- and F-coronal polarized brightness, while $I_{\text{unpol},\lambda}$ contains the unpolarized solar disk light coming from the diffraction of the external occulter.

The diffraction and the vignetting of the occulter depend on the radial distance from the Sun as shown in Figure 2. They are determined by the optical simulations of *CODEX*. The QE_λ used in the calculation is measured with the flight model of the *CODEX* camera.

The number of electrons in a pixel is converted to a digital number to which the noise from various sources is added. The digital number of the recorded signal s_θ can be expressed as

$$s_\theta = (e_\theta t_{\text{exp}} + \text{shot}_e + \text{dark}_e t_{\text{exp}} + \text{readout}_{\text{rms,e}})/g, \tag{2}$$

where t_{exp} is the exposure time, and g is the gain of the camera. The term shot_e describes the shot noise, the term $\text{dark}_e t_{\text{exp}}$ is the dark noise, and the term $\text{readout}_{\text{rms,e}}$ is the readout noise. The sum of the signal $e_\theta t_{\text{exp}}$ and the shot noise, or so called photon noise, is modeled by a Poisson distribution. The Poisson distribution can be treated as a Gaussian distribution in the case of large samplings. However, the F-coronal signal is too small to be treated as a Gaussian. The dark current ($\text{dark}_e t_{\text{exp}}$) is a noise generated by the thermal energy in a pixel. The dark current also follows a Poisson statistics. The readout noise is generated by the imperfection of the electron counting in the output amplifier, and, therefore, it does not depend on time. The readout noise is treated as a Gaussian distribution with the standard deviation of $\text{readout}_{\text{rms,e}}$ centered at zero.

Note that the readout of each pixel in the CMOS sensor is different from each other because each pixel of the CMOS sensor has several transistors and gain, unlike the charge-coupled devices (CCD) sensor. But the deviations of the gain, the dark current, and the readout noise of each pixel in the sensor could not be considered in this study because the deviations are not characterized yet. The deviations will be corrected by on-ground flat field calibration.

Figure 3 displays the number of the recorded electrons along the radial distance from the Sun using a 90-second exposure time. The number of electrons at $3\,R_\odot$ reaches 625, which is appropriate for the full well depth of the sensor. The signal is mostly dominated by the (unpolarized) F-coronal brightness. In the NBF case, the dark current overwhelms other signals. We use a 90-second exposure time to avoid the effect of probable image rotation during the tracking.
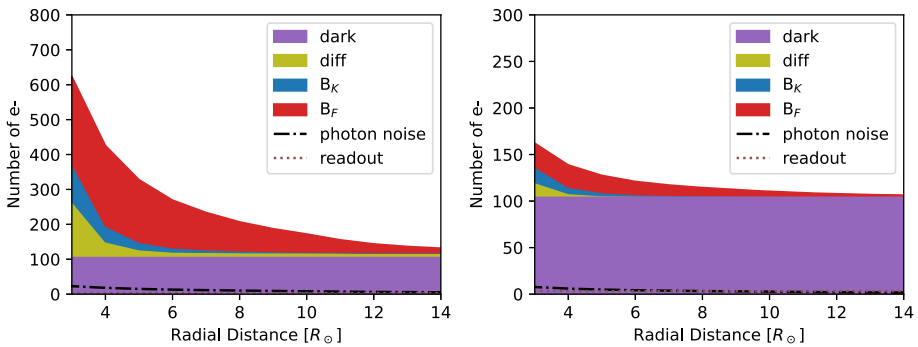
Figure 3 Recorded electrons with a broadband filter centered at 393.5 nm (left panel) and a narrow band filter centered at 393.55 nm (right panel).

As a result of the above calculations, we obtain the signals of all four polarization pixels, i.e., $s_{0°}$, $s_{45°}$, $s_{90°}$, and $s_{135°}$. Then, the polarized brightness signal pBs_f and the total brightness signal tBs_f of specific pixels transmitted to a specific bandpass filter can be calculated as in Reginald et al. (2017)

$$pBs_f = \sqrt{(s_{0°} - s_{90°})^2 + (s_{45°} - s_{135°})^2}, \tag{3}$$

$$tBs_f = \frac{1}{2}(s_{0°} + s_{45°} + s_{90°} + s_{135°}). \tag{4}$$

We assume that the dark current and readout noise are removed from the post-processed data, and only the random deviation remains. We also assume that part of $I_{unpol,\lambda}$ coming from the unpolarized solar disk light diffracted from the external occulter is subtracted, except its random deviation.

By calculating Equation 3 and Equation 4, we can obtain tBs_f and pBs_f as follows

$$pBs_f = \int (\frac{t_f * t_{optics}}{E_{ph,\lambda}} * QE_\lambda * A_{ap} * \Omega_{pixel})(1 - \frac{1}{ext_{pol}})(I_{t,\lambda} - I_{r,\lambda})\frac{t_{exp}}{g} \, d\lambda,$$

$$tBs_f = \int (\frac{t_f * t_{optics}}{E_{ph,\lambda}} * QE_\lambda * A_{ap} * \Omega_{pixel})(1 + \frac{1}{ext_{pol}})(I_{t,\lambda} + I_{r,\lambda} + I_{unpol,\lambda})\frac{t_{exp}}{g} \, d\lambda.$$

Assuming that pB_K and pB_F do not cancel out each other, we can express the observed signal as

$$pBs_f = \int R_{f,\lambda} \epsilon^- (pB_K(\lambda) + pB_F(\lambda)) \, d\lambda, \tag{5}$$

$$tBs_f = \int R_{f,\lambda} \epsilon^+ (tB_K(\lambda) + tB_F(\lambda)) \, d\lambda, \tag{6}$$

where $R_{f,\lambda}$ is a response function of the instrumentation

$$R_{f,\lambda} = \frac{t_f * t_{optics}}{E_{ph,\lambda}} * QE_\lambda * A_{ap} * \Omega_{pixel} * \frac{t_{exp}}{g},$$

and ϵ^- and ϵ^+ are

$$\epsilon^- = (1 - \frac{1}{ext_{\text{pol}}}),$$

$$\epsilon^+ = (1 + \frac{1}{ext_{\text{pol}}}).$$

We also assume that the degrees of linear polarization for both the K- and F-coronal spectra are independent of the wavelength. This assumption is reasonable for the K-coronal spectrum because Thomson scattering is almost wavelength-independent within a short wavelength range. For the F-coronal spectrum, the Mie scattering is also not very sensitive to the wavelength within the relatively short wavelength range.

The degree of linear polarization for K- (D_K) and F-corona (D_F) are expressed as

$$D_K = pB_K(\lambda) / tB_K(\lambda),$$

$$D_F = pB_F(\lambda) / tB_F(\lambda).$$

The D_F is the parameter we want to obtain from the *CODEX* observations. Now Equation 5 and Equation 6 become

$$pBs_f = D_K \int R_{f,\lambda} \epsilon^- tB_K(\lambda) \, d\lambda + D_F \int R_{f,\lambda} \epsilon^- tB_F(\lambda) \, d\lambda,$$

$$tBs_f = \int R_{f,\lambda} \epsilon^+ tB_K(\lambda) \, d\lambda + \int R_{f,\lambda} \epsilon^+ tB_F(\lambda) \, d\lambda.$$

Because the K-coronal spectrum varies slowly over the wavelength, we can approximately describe the K-coronal spectrum as a linear function of λ. If the response function is symmetric with respect to the central wavelength of the filter λ_0, we can simplify the notation

$$\int R_{f,\lambda} tB_K(\lambda) \, d\lambda \simeq \bar{R}_f \, tB_K(\lambda_0),$$

$$\int R_{f,\lambda} pB_K(\lambda) \, d\lambda \simeq \bar{R}_f \, pB_K(\lambda_0),$$

where $\bar{R}_f$ is the constant of the response of a specific filter

$$\bar{R}_f = \int R_{f,\lambda} \, d\lambda.$$

$\bar{R}_f$ is only proportional to the bandwidth (w_f) because other parameters are constant or vary slowly over the wavelength

$$\frac{\bar{R}_b}{\bar{R}_n} = \frac{w_b}{w_n}.$$

The observed pBs and tBs of the BBF and the NBF can be expressed as

$$pBs_n = \epsilon^- D_K \bar{R}_n \, tB_K(\lambda_0) + \epsilon^- D_F \int R_{n,\lambda} \, tB_F(\lambda) \, d\lambda,$$

$$pBs_b = \epsilon^- D_K \bar{R}_b \, tB_K(\lambda_0) + \epsilon^- D_F \int R_{b,\lambda} \, tB_F(\lambda) \, d\lambda,$$

$$tBs_n = \epsilon^+ \bar{R}_n \, tB_K(\lambda_0) + \epsilon^+ \int R_{n,\lambda} \, tB_F(\lambda) \, d\lambda,$$

$$tBs_b = \epsilon^+ \bar{R}_b \, tB_K(\lambda_0) + \epsilon^+ \int R_{b,\lambda} \, tB_F(\lambda) \, d\lambda,$$

where subscripts n and b indicate NBF and BBF, respectively. By substituting $\int R_{n,\lambda} \, tB_F(\lambda) \, d\lambda$, $\int R_{f,\lambda} \, tB_F(\lambda) \, d\lambda$ and $tB_K(\lambda_0)$ from the above equations and combining them into one, D_F can be expressed as

$$D_F = \left(\frac{ext_{pol} + 1}{ext_{pol} - 1} \right) \left(\frac{w_b \, pBs_n - w_n \, pBs_b}{w_b \, tBs_n - w_n \, tBs_b} \right). \tag{7}$$

In Equation 7, the first fraction contains the effect of the extinction ratio. $w_b \, pBs_n$ and $w_b \, tBs_n$ of the second fraction represent the brightness of the absorption line added to the continuum, while $w_n \, pBs_b$ and $w_n \, tBs_b$ represent only the brightness of the continuum. That is, the D_F is the degree of linear polarization at the absorption line subtracting the degree of linear polarization of the continuum. We note that it is impossible to distinguish D_F and D_K if the denominator of the second term is zero. This can happen if there is no absorption line in the observed spectrum. In actual observations, we will disregard the pixels where the second term is close to zero.

We remark that one of the critical assumptions of this study is that the signal of pB_K and pB_F do not cancel when we derive Equations 5 and 6. This assumption is critical because there is no reason for the K- and F-corona to have the same directional polarizations. In addition, we may not notice even though there exist cancellations in the observational data if we use only the results of these two filters. We can resolve the uncertainties of the cancellations using the observational result of D_K and pB_K of the other BBFs (Reginald, Newmark, and Rastaetter, 2021).

4. Monte-Carlo Calculations and Analysis

We calculate the signals of each pixel of the *CODEX* with the NBF and the BBF using Monte-Carlo methodology by computing 10 000 samples for uncertain parameters: shot noise, dark current, and readout noise. Because the combined uncertainty caused by the noise is so large, we consider stacking and binning the images to increase the signal-to-noise ratio. We assume that the post-processed data – dark current and flat field removal – are accurately obtained, except their noise. After calculating the signal, we extract D_F from the signals with two filters following Equation 7.

Figure 4 shows the change of D_F according to the number of stacked images at $7 R_\odot$ when we use NBF with a 393.55 nm central wavelength and 1.4 nm bandwidth. We note that the input value of the calculation includes D_F from Koutchmy and Lamy (1985). D_F is dominated by noise in a single image. By stacking images, the value approaches the value of the input D_F (Koutchmy's D_F). The standard deviation decreases by stacking more images. Thus, we may detect about 1.6% of the polarization with a 2σ accuracy by stacking about 30 000 images (or pixels). Note that the spatial pixel resolution of $1 R_\odot$ can be achieved by binning 75×75 super-pixels (equivalent to stacking 5 625 images). Then the 2σ accuracy

Figure 4 D_F variation according to the number of stacked images at $7\,R_\odot$ in the case of (a) no pB_F, (b) 1.0×, (c) 2.0×, and (d) 3.0× of Koutchmy's result. Considering that the fraction of the polarization at $7\,R_\odot$ is about 1.6% in their model (dash-dot line in the panel (b)), the percentage of the polarization of the F-corona would be about 0%, 1.6%, 3.2%, and 4.8%, respectively. The gray regions represent the 2σ error range of the result.
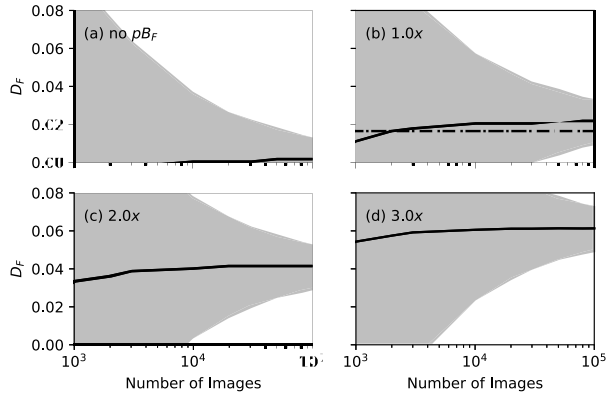
Figure 5 δD_F by changing the bandwidth and the central wavelength of the narrow bandpass filter at $7\,R_\odot$. The zero line shift is at 393.55 nm.
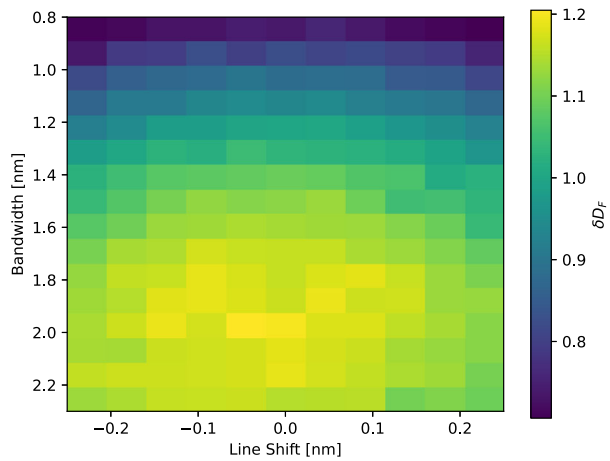
can be achieved by stacking about six binned images. The spatial pixel resolution can be enhanced by stacking more images.

We also note that the measured D_F (black solid line in Figure 4 (b)) exceeds the expected (or input) D_F (black dash-dot line) after stacking more than 2 000 images. This may be due to the assumption of the K-coronal spectrum as a linear function of λ, as shown by Equation 7.

To determine the appropriate central wavelength (λ_n) and the bandwidth (w_n) of the NBF, we define a value of the difference of the F-coronal degree of linear polarization (δD_F) between the cases of no pB_F $D_{F,0\times}$ and the cases of 1.0× of Koutchmy's result $D_{F,1\times}$ as

$$\delta D_F = \frac{D_{F,1\times} - D_{F,0\times}}{2\sigma_{1\times}}, \tag{8}$$

where $D_{F,0\times}$ and $D_{F,1\times}$ are the result of Equation 7 with the F-coronal model of no pB_F and 1.0× of Koutchmy's result, and $\sigma_{1\times}$ is the standard deviation of $D_{F,1\times}$. The bandwidth of the NBF can be selected where δD_F is larger than unity. Then we can distinguish D_F of 1.6% from that of 0% with a 2σ accuracy.

Figure 5 presents the variation of δD_F with 75×75 super-pixel binning and six image stacking, by changing the central wavelength λ_n and the bandwidth w_n of NBF. δD_F is

Figure 6 D_F variation over the radial distances from the Sun in the case of (a) no pB_F, (b) 1.0×, (c) 2.0×, and (d) 3.0× of Koutchmy's result. The data are calculated by binning 75 × 75 super-pixels and stacking 18 images. The D_F is overestimated compared to the expected values (see a dash-dot line of (b)) due to the large noise and the assumptions of the model. The gray regions also represent the 2σ error range.
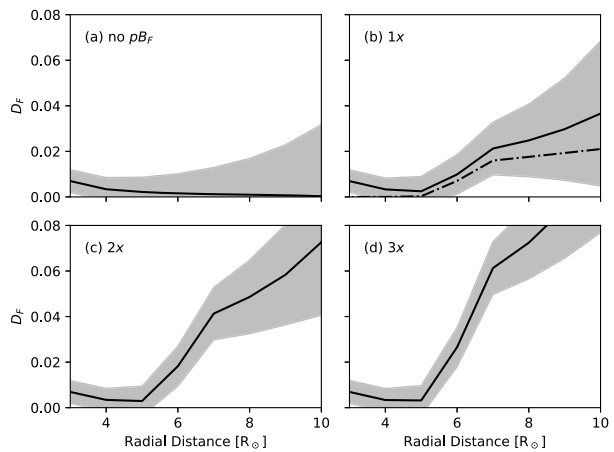
maximum at $\lambda_n = 393.55$ nm and $w_n = 1.8 - 2.0$ nm. Although δD_F peaks at $1.8 - 2.0$ nm in this calculation, we chose 1.4 nm as w_n of NBF based on the estimated specification of the CMOS camera such as dark current, the readout noise, or the QE. Larger w_n could be more efficient for extracting pB_F from pB_K considering the additional noise sources such as the imperfect transmission profiles or the shifted central wavelength of the custom-made bandpass filter. However, the expected difference in its performance is not significantly large.

We present the D_F variation and its deviation along the radial distance from the Sun in Figure 6. As in Koutchmy's model, pB_F increases from $5\,R_\odot$ outward, but because the signal decreases, the deviation increases. As shown in Figure 4, we distinguish 1.6% of pB_F from 0% at $7\,R_\odot$ with 2σ accuracy after stacking 18 binned images. Under $6\,R_\odot$, it is hard to achieve 2σ accuracy due to the higher noise. Stacking more images is necessary to distinguish Koutchmy's pB_F. From $3\,R_\odot$ to $5\,R_\odot$, about 0.7% of D_F is recorded, which is expected to be zero. This deviation is due to the assumption of the K-coronal spectrum as a linear function of the wavelength when we derive Equation 7. As the spectrum of pB_K has a small valley, as shown in Figure 1, part of pB_K contaminates the result of D_F. When D_F is higher than 2× of Koutchmy's result, it becomes distinguishable with high clarity from around $5\,R_\odot$ and beyond.

5. Summary and Discussion

The present paper shows that the F-coronal polarized brightness, pB_F, can be measured by observations using a 1.4 nm-width narrow bandpass filter (NBF) and a 10 nm-width broad bandpass filter (BBF) that will be installed on the Coronal Diagnostic Experiment (*CODEX*). After stacking and binning the observed images, we expect that *CODEX* would provide the radial profiles of the degree of linear polarization of the F-coronal light (D_F), which has not been investigated well so far. Our results of the F-coronal can also be used to correct the contamination of the polarized brightness of the K-corona (pB_K), which is the main science objective of *CODEX*.

The 2-dimensional distribution of pB_F can be associated with the origin of the F-corona. The pB_F can be observed, and it becomes stronger approaching the inner corona if part of the pB_F is generated by the interplanetary dust particles (IDPs) near the Earth. This is because

IDPs near the Earth can generate strong forward scattering. To the best of our knowledge, there exist only few studies on pB_F in the low ($< 5\,R_\odot$) solar corona during TSEs or in space because pB_F is too small to be measured during TSEs or ground observations. We expect that *CODEX* would provide us a hint on the distribution of the F-corona as well as its variation with time.

Near-sun IDPs, which can be revealed using these F-coronal observations, are likely one of the crucial contributors to space weather. Coronal mass ejections or the solar wind may interact with IDPs by charging and discharging them. Then the solar wind and CMEs can be accelerated or decelerated. Additionally, the amount and the composition of the K- and F-corona extracted from the *CODEX* observations may be important in the energy transport in the interplanetary medium (Morgan and Habbal, 2007).

In this study, we calculated the radial profiles based on the assumption of Koutchmy's polarized brightness of the F-corona, pB_F. The shape of the radial profiles of the signal or pB_F may change at $5\,R_\odot$, assuming this pB_F. As the evaporating or melting temperature of the dust depends on its composition, as well as the size and shape of particles, the transition may not be as sharp as expected by Koutchmy and Lamy (1985). To interpret pB_F from *CODEX*, it may be necessary to perform further simulations with various physical parameters.

Declarations

Competing interests The authors declare no competing interests.

References

ASTM Committee E21 on Space Simulation and Applications of Space Technology: 2006, Standard solar constant and zero air mass solar spectral irradiance tables ASTM International.

Baumbach: 1937, Strahlung, Ergiebigkeit und Elektro- nendichte der Sonnenkorona. *Astron. Nachr.* **263**, 120.

Blackwell, D.E., Petford, A.D.: 1966, Observations of the 1963 July 20 solar eclipse. II, The electron density in the solar corona in the region $5 < R/R < 16$ obtained from measurements of Fraunhofer line depth and the polarization of the F corona. *Mon. Not. Roy. Astron. Soc.* **131**, 399. DOI. ADS.

Boe, B., Habbal, S., Downs, C., Druckmüller, M.: 2021, The color and brightness of the F-corona inferred from the 2019 July 2 total solar eclipse. *Astrophys. J.* **912**, 44. DOI. ADS.

Burtovoi, A., Naletto, G., Dolei, S., Spadaro, D., Romoli, M., Landini, F., De Leo, Y.: 2022, Measuring the F-corona intensity through time correlation of total and polarized visible light images. *Astron. Astrophys.* **659**, A50. DOI. ADS.

Cho, K., Chae, J., Lim, E.-k., Cho, K.-s., Bong, S.-C., Yang, H.: 2016, A new method to determine temperature of CMES using a coronagraph filter system. *J. Korean Astron. Soc.* **49**, 45. DOI. ADS.

Cho, K.-S., Yang, H., Lee, J.-O., Bong, S.-C., Kim, J., Choi, S., Park, J., Cho, K., Baek, J.-H., Kim, Y.-H., Park, Y.-D.: 2020, Toward a next generation solar coronagraph: diagnostic coronagraph experiment. *J. Korean Astron. Soc.* **53**, 87. DOI. ADS.

Hanaoka, Y., Sakai, Y., Takahashi, K.: 2021, Polarization of the corona observed during the 2017 and 2019 total solar eclipses. *Solar Phys.* **296**, 158. DOI. ADS.

Kimura, H., Mann, I.: 1998, Brightness of the solar F-corona. *Earth Planets Space* **50**, 493. DOI. ADS.

Koutchmy, S., Lamy, P.L.: 1985, The F-corona and the circum-solar dust evidences and properties (ir). In: Giese, R.H., Lamy, P. (eds.) *IAU Colloq. 85: Properties and Interactions of Interplanetary Dust* **63**. DOI. ADS.

Lamy, P., Llebaria, A., Boclet, B., Gilardy, H., Burtin, M., Floyd, O.: 2020, Coronal photopolarimetry with the LASCO-C2 coronagraph over 24 years [1996 - 2019]. *Solar Phys.* **295**, 89. DOI. ADS.

Lasue, J., Levasseur-Regourd, A.-C., Renard, J.-B.: 2020, Zodiacal light observations and its link with cosmic dust: a review. *Planet. Space Sci.* **190**, 104973. DOI.

Leblanc, Y., Dulk, G.A., Bougeret, J.-L.: 1998, Tracing the electron density from the corona to 1 au. *Solar Phys.* **183**, 165. DOI. ADS.

Llebaria, A., Lamy, P., Gilardy, H., Boclet, B., Loirat, J.: 2021, Restoration of the K and F components of the solar corona from LASCO-C2 images over 24 years [1996 - 2019]. *Solar Phys.* **296**, 53. DOI. ADS.

Mann, I.: 1998, Zodiacal cloud complexes. *Earth Planets Space* **50**, 465. DOI. ADS.

Mann, L., MacQueen, R.M.: 1993, The solar F-corona at 2.12 pin: calculations of near-solar dust in comparison to 1991 eclipse observations. *Astron. Astrophys.* **275**, 293. ADS.

Mann, I., Kimura, H., Biesecker, D.A., Tsurutani, B.T., Grün, E., McKibben, R.B., Liou, J.-C., MacQueen, R.M., Mukai, T., Guhathakurta, M., Lamy, P.: 2004, Dust near the sun. *Space Sci. Rev.* **110**, 269. DOI. ADS.

Mie, G.: 1908, Beiträge zur Optik trüber Medien, speziell kolloidaler Metallösungen. *Ann. Phys.* **330**, 377. DOI.

Morgan, H., Cook, A.C.: 2020, The width, density, and outflow of solar coronal streamers. *Astrophys. J.* **893**, 57. DOI. ADS.

Morgan, H., Habbal, S.R.: 2007, The long-term stability of the visible F corona at heights of 3-6 R$_\odot$. *Astron. Astrophys.* **471**, L47. DOI. ADS.

Ragot, B.R., Kahler, S.W.: 2003, Interactions of dust grains with coronal mass ejections and solar cycle variations of the F-coronal brightness. *Astrophys. J.* **594**, 1049. DOI. ADS.

Reginald, N., Newmark, J., Rastaetter, L.: 2021, Statistical error analysis on white-light filter ratio experiments to measure electron parameters. *Solar Phys.* **296**, 146. DOI. ADS.

Reginald, N., Gopalswamy, N., Yashiro, S., Gong, Q., Guhathakurta, M.: 2017, Replacing the polarizer wheel with a polarization camera to increase the temporal resolution and reduce the overall complexity of a solar coronagraph. *J. Astron. Telesc. Instrum. Syst.* **3**, 1. DOI.

van de Hulst, H.C.: 1947, Zodiacal light in the solar corona. *Astrophys. J.* **105**, 471. DOI. ADS.

van de Hulst, H.C.: 1950, The electron density of the solar corona. *Bull. Astron. Inst. Neth.* **11**, 135. ADS.

Yang, H., Ishiguro, M.: 2015, Origin of interplanetary dust through optical properties of zodiacal light. *Astrophys. J.* **813**, 87. DOI. ADS.

Zubko, E., Shkuratov, Y., Kiselev, N.N., Videen, G.: 2006, DDA simulations of light scattering by small irregular particles with various structure. *J. Quant. Spectrosc. Radiat. Transf.* **101**, 416. Light in Planetary Atmospheres and Other Particulate Media. DOI.

Authors and Affiliations

Heesu Yang[1] · **Kyuhyoun Cho**[2,3] · **Su-Chan Bong**[1] · **Seonghwan Choi**[1] · **Maria S. Madjarska**[4,5] · **Yeon-Han Kim**[1] · **Nelson Reginald**[6] · **Jeffrey Newmark**[6]

✉ H. Yang
hsyang@kasi.re.kr

K. Cho
cho@baeri.org

S.-C. Bong
scbong@kasi.re.kr

S. Choi
shchoi@kasi.re.kr

M.S. Madjarska
madjarska@mps.mpg.de

Y.-H. Kim
yhkim@kasi.re.kr

N. Reginald
nelson.l.reginald@nasa.gov

J. Newmark
jeffrey.newmark@nasa.gov

1   Korea Astronomy and Space Science Institute, Daejeon 34055, Republic of Korea

2   Bay Area Environmental Research Institute, NASA Research Park, Moffett Field, CA 94035, USA

3   Lockheed Martin Solar & Astrophysics Laboratory, 3251 Hanover Street, Palo Alto, CA 94304, USA

4   Max-Planck-Institute for Solar System Research, Justus-von-Liebig-Weg 3, 37077 Göttingen, Germany

5   Space Research and Technology Institute, Bulgarian Academy of Sciences, Acad. Georgy Bonchev Str., Bl. 1, 1113, Sofia, Bulgaria

6   NASA Goddard Space Flight Center, Greenbelt, MD 20771, USA